

Stable Aqueous Solutions of Naked Titanate Nanotubes

Lucio Zennaro,^[b] Massimiliano Magro,^[c] Fabio Vianello,^[c] Adelio Rigo,^[b] Gino Mariotto,^[d] Marco Giarola,^[d] Elena Froner,^[a] and Marina Scarpa*^[a]

Aqueous solutions of naked nanotubes with Ti concentration up to 10 mM are obtained by hydrothermal synthesis followed by extensive ultrasound treatment. The morphology, surface characteristics, and solution behavior of the solubilized nanotubes are investigated. The time course of the solubilization process driven by ultrasound follows a first-order kinetic law and is mediated by the competition between Na⁺ and H⁺ for surface sites. The dynamics of interaction with small cations

(i.e. the sodium ion) is studied by nuclear magnetic resonance spectroscopy and is demonstrated to be a multifaced process, since Na⁺ is in part free to exchange between the binding sites on nanotubes and the bulk and in part is confined to slowly exchanging nanotube sites. The aqueous titanate nanotube solutions are stable for months, thus opening new perspectives for the use of this material in drug delivery and in homogeneous photocatalysis.

1. Introduction

Nanotubes derived from TiO₂ are attracting increasing interest because of their characteristic properties, such as a high aspect ratio, the mildly reactive nature of their surface, and the semiconductor bandgap that can be tuned from the UV to the visible range.^[1] Accordingly, after the pioneering work of Hoyer,^[2] the rate of publication of papers and patents dealing with titanate nanotubes has been continuously increasing.^[3,4] The current research activities are mainly aimed at understanding the physical and chemical features of titanate nanotubes. However, titanate nanotubes can also find versatile applications and the exploitation of this outstanding material in the biomedical, photochemical, electrical, and environmental fields appears promising.^[5] Recently, two topics have emerged: titanate nanotubes as an efficient system for environmental depollution^[6] and titanate nanotubes as a biomedical tool.^[7,8] Titanium oxide is in fact an excellent photocatalyst. In particular, it oxidizes toxic organic compounds on addition to contaminated water and illumination by mild UV light. This is a clean

process for contaminant removal since, besides atmospheric oxygen, no other reagent is needed for the reaction to proceed.^[9] Nanostructuring of titanium oxides enhances the photocatalytic efficiency and titanate nanotubes suitably doped can also be excited in the visible range.^[10–14] Biomedical applications of titanates are encouraged by the low toxicity of titanium and titanium alloys, which are traditionally used for bone implants and prosthesis coatings. Titanate nanotube surfaces offer advantages compared with flat TiO₂ surfaces, since cell adhesion is favored and processes such as bone growth are stimulated.^[15] Finally, the capsule-shaped geometry of nanotubes suggests their use as drug-delivery vehicles and imaging enhancers.^[16,17]


Up to now the majority of the experimental proofs of the titanate nanotube performances have been obtained by using titanate nanotube assemblies, or layers or powders dispersed in solvents. Titanate nanotubes are usually synthesized by electrochemical anodization,^[18] template-assisted electrochemical deposition,^[2] atomic layer deposition,^[19] the sol-gel technique,^[20] or hydro/solvothermal synthesis.^[3,21] Ordered layers or powders obtained by means of these synthesis methods are practically insoluble in water (a solubility of 0.2 mg L⁻¹ has been reported).^[22] These titanate nanotube phases, in particular the ordered solid titanate nanotube structures, show exceptional features for some applications (such as for solar cells, heterogeneous catalysis, filtration devices). However, in some cases a great advantage will be obtained by the homogeneous dispersion of the titanate nanotubes in the aqueous environment, for example, if titanate nanotubes are used for drug delivery into the systemic circulation or for homogeneous catalysis. High water solubility is essential for the successful exploitation of titanate nanotubes in water depollution, in which optimum photocatalytic performances, such as absence of light scattering effects, are necessary. Conversely, these effects are reported to be quite high in titanate aqueous suspensions. Functionalization processes have been proposed to overcome

[a] Dr. E. Froner, Prof. M. Scarpa
Dipartimento di Fisica
Università di Trento and Istituto Nazionale di Biostrutture e Biosistemi
via Sommarive 14, 38123 Povo Trento (Italy)
Fax: (+39)0461282967
E-mail: marina.scarpa@unitn.it

[b] Prof. L. Zennaro, Prof. A. Rigo
Dipartimento di Medicina Molecolare
Università di Padova and Istituto Nazionale di Biostrutture e Biosistemi
via G. Colombo 3, 35100 Padova (Italy)

[c] Dr. M. Magro, Prof. F. Vianello
Dipartimento di Biomedicina Comparata ed Alimentazione
Università di Padova
via G. Colombo 3, 35100 Padova (Italy)

[d] Prof. G. Mariotto, Dr. M. Giarola
Dipartimento di Informatica
Università di Verona
Strada le Grazie 15, 37134 Verona (Italy)

 Supporting information for this article is available on the WWW under <http://dx.doi.org/10.1002/cphc.201300292>.

this drawback.^[23,24] However, the organic coating can introduce unwanted changes of the titanate nanotube dimensions and properties. Moreover, the organic coating itself can be degraded during titanate photocatalysis whereas biomedical applications necessitate that the surface reactive groups of titanate nanotubes (namely hydroxyl groups) are preserved to bind bioactive agents, such as targeting molecules or growth factors. Finally, in view of large-scale utilization of the titanate nanotubes, expensive coating procedures performed only to solubilize the starting nanomaterial should be avoided. Therefore, preparation and utilization of concentrated, highly active, and clear titanate nanotube aqueous solutions might be helpful in solving some of the above-mentioned problems.

Herein, we report a simple procedure of hydrothermal synthesis of titanate nanotubes followed by ultrasound treatment, which permits stable and concentrated titanate nanotube aqueous solutions to be obtained. As far as we know it is the first time that stable solutions of naked titanate nanotubes have been prepared. Morphological characterization of these soluble titanate nanotubes has been performed. The relationships between solubility, structure, and the solvent-exposed interface, that is, the presence of surface sites at which Na^+ ions are confined, have been investigated by means of optical and vibrational spectroscopies and by solution nuclear magnetic resonance spectroscopy.

2. Results and Discussion

2.1. Dynamics of the Solubilization Process

More than 80% of the washed and dried titanate nanostructures was brought into solution by extensive ultrasound treatment in distilled water. The final solutions so obtained were characterized by a pH value close to neutrality and an electrical conductivity of less than 20 μS .

The trend over time of the solubilization process of the titanate powder assisted by ultrasound was monitored by the absorbance increase at 245 nm and is shown in Figure 1. At this wavelength the absorbance reaches a maximum. The absorbance increase was fitted satisfactorily to a first-order kinetic law and a kinetic rate constant of $(1.7 \pm 0.3) \times 10^{-3} \text{ min}^{-1}$ was calculated. The titanium content in the final solutions was measured according to the procedure reported in the Experimental Section and was found to be as high as 100 mmol TiO_2 . In some cases the clear solutions were lyophilized and all the dry material was brought again into solution by sonication in distilled water. This second solubilization process followed a first-order kinetic law, but in this case the process was faster (the rate constant was $(5.5 \pm 0.7) \times 10^{-3} \text{ min}^{-1}$). Transmission electron mi-

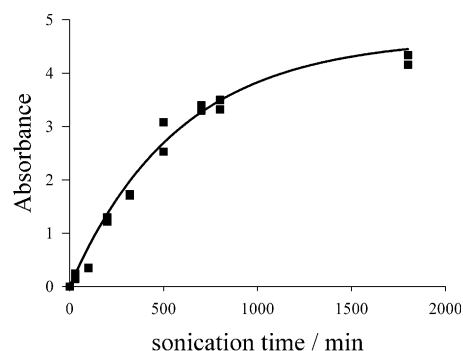


Figure 1. Absorbance of titanate nanotube solutions at various times of ultrasound treatment. The titanate nanotubes, suspended in distilled water, underwent ultrasound treatment at 400 W and 65 °C. Solid line: first-order fitting ($k = (1.7 \pm 0.3) \times 10^{-3} \text{ min}^{-1}$).

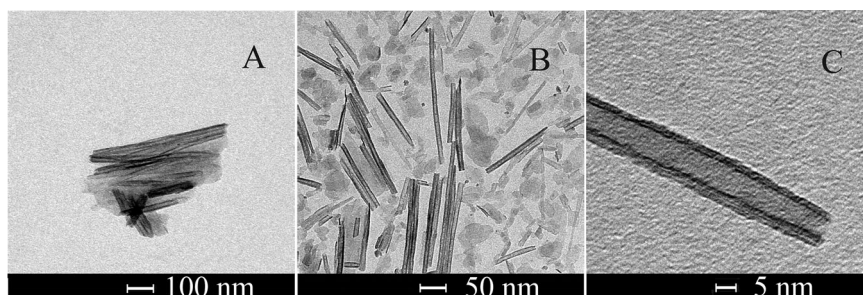


Figure 2. TEM images of titanate nanotubes. Nanotubes before (A) and after (B) ultrasound treatment. C) Typical open-ended nanotube after sonication. A small drop of a dilute solution of nanotubes was deposited on the Cu grid.

croscopy (TEM) images clearly show nanotubular-shaped structures (see Figure 2), so we designate them as titanate nanotubes. Sonication may fracture some of the titanate nanotubes along their length. However, according to the TEM images the nanotubes deposited from the clear solutions were on average 200 nm long, as shown by the length distribution reported in Figure 3.

The ultrasound treatment was also carried out in the presence of 1 mmol NaCl, or 1 mmol NaCl plus 1 mmol NaOH, or 1 mmol NaCl plus 1 mmol HCl. Although NaCl alone did not induce effects on the rate of solubilization ($k = 1.52 \times 10^{-3} \text{ min}^{-1}$), the ad-

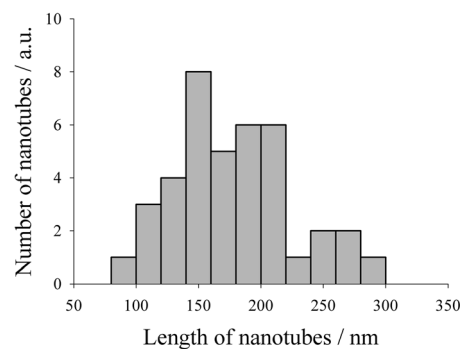


Figure 3. Length distribution of titanate nanotubes present in solution after 2400 min of ultrasound treatment.

dition of NaCl plus NaOH increased the rate by about five times ($k=10.4\times 10^{-3}\text{ min}^{-1}$). Conversely, the addition of HCl decreased the initial rate of solubilization by about one order of magnitude. This behavior suggests that Na^+ binding sites on the nanotube surface are present, and the interaction of the nanotubes with the aqueous solution is mediated by the competition of Na^+ with H^+ for the occupancy of these sites. The nanotube solutions obtained by the exhaustive ultrasound process were stable for more than 12 months.

2.2. Optical Characterization of the Solubilized Titanate Nanotubes

The solid trace in Figure 4 shows the absorption spectrum of solutions of nanotubes obtained by ultrasound dispersion in

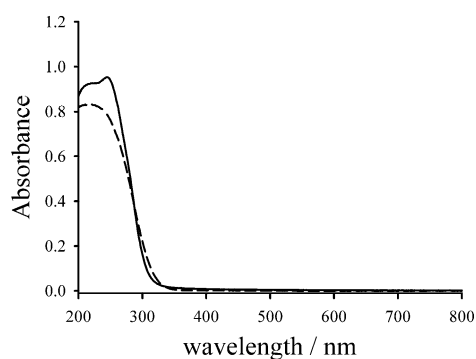


Figure 4. UV/Vis spectra of aqueous solutions of titanate nanotubes. (—): spectrum of aqueous solution of sodium titanate nanotubes after centrifugation at 10000 g (pH 6.91). (---): spectrum of a solution of TiO_2 nanoparticles (pH 2.1).

distilled water after 20 min of centrifugation (at $10^4 g$), whereas the dashed-line trace is the spectrum of a solution of TiO_2 nanoparticles reported for comparison. The titanate nanotube spectrum is notably different from that of the nanoparticles supporting a different nanostructure of TiO_2 . Notably, after 2 h of centrifugation of titanate nanotubes at $4\times 10^4 g$, no significant spectral change was observed with respect to the spectrum shown in Figure 4. Titanate nanotubes have a characteristic maximum absorbance at 245 nm, which undergoes a red-shift of about 3 nm above pH 8 (data not shown). On the basis of the titanium content of the solutions, determined as peroxy-titanate complex,^[25] a molar extinction coefficient of $(9.5\pm 0.1)\times 10^3\text{ mol}^{-1}\text{ Lcm}^{-1}$ at 245 nm was calculated for titanate nanotubes, whereas the nanoparticle molar extinction coefficient was $(6\pm 0.1)\times 10^3\text{ mol}^{-1}\text{ Lcm}^{-1}$ at 230 nm.

2.3. Morphological Characterization of Soluble Titanate Nanotubes

The TEM images of the as-prepared titanate nanotubes (i.e. the material obtained by the hydrothermal process before the ultrasound treatment) show the presence of large aggregates, as visible in Figure 2A. Figure 2B shows a representative TEM high-magnification image of the titanate nanotubes deposited

from the aqueous solution after ultrasound treatment and drying on a TEM grid. The images show the presence of isolated titanate nanotubes of nearly uniform diameter. All the titanate nanotubes are open ended (see Figure 2C). The outer diameter ranges from 8 to 10 nm and the inner diameter is about 4 nm, with an interlayer spacing of 0.8 nm. The nanotubes are some hundred nanometers in length. Similar results were obtained when a drop of 1:1000 diluted titanate nanotube solution was deposited on a mica surface and observed by atomic force microscopy (AFM). Tapping mode AFM allows the acquisition of images under mild conditions; in particular, the hydration layer of the deposited nanomaterial is preserved. Also in this case, only single titanate nanotubes were observed and an average nanotube diameter of $(8\pm 1)\text{ nm}$ was measured (see Figure 5).

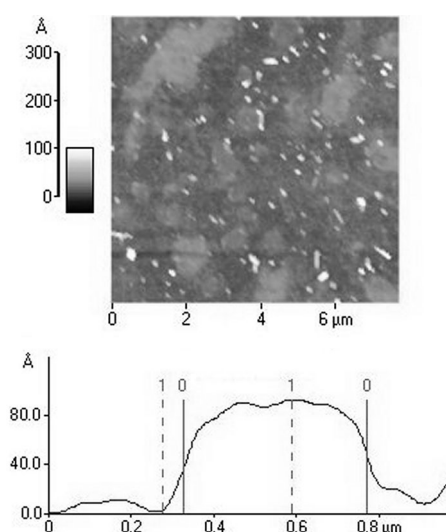


Figure 5. AFM image and height profile of nanotubes. The titanate nanotube solution was deposited on a mica surface and left to dry. The instrumental settings were: intermittent contact head, $20\times 20\text{ }\mu\text{m}$ scan size, 512×512 points per line, 1 Hz scan rate, tapping mode technique.

2.4. ^{23}Na NMR Spectroscopy of Titanate Nanotube Solutions

The magnetic resonance of ^{23}Na was investigated to obtain insights into the Na^+ confined in the nanotubes or present in the surrounding environment. A representative spectrum of ^{23}Na in titanate nanotube neutral solutions is reported in Figure 6. The single peak of Figure 6 is characterized by a half-height line width ($\Delta\nu_{1/2}$) of 390 Hz. This value is an order of magnitude higher than the line width of 1 mM aqueous NaCl, which is about 16 Hz. A calibration curve of the NMR peak area versus the concentration of Na^+ was obtained by using standardized solutions of NaCl (data not shown). This curve was used to determine the concentration of Na^+ in the titanate nanotube solution and in the same sample after destruction of nanotubes by H_2SO_4 (as reported in the Experimental Section). From the measured Na^+ and Ti concentrations we calculated an atomic ratio Na/Ti of 0.046 and 0.083 before and after H_2SO_4 treatment, respectively. These data indicate that about 50% of the Na^+ in titanate nanotube solutions is NMR

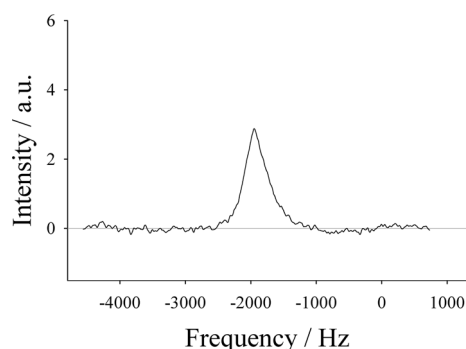


Figure 6. ^{23}Na NMR spectrum of a titanate nanotube aqueous solution. The titanate nanotube concentration was 32 mM TiO_2 equivalents. The instrumental carrier frequency was used as reference and arbitrarily set to 0.

silent, probably because it is strongly immobilized ($\Delta\nu_{1/2} > 2000$ Hz). The resonance of the remaining Na^+ is still large ($\Delta\nu_{1/2} = 390$ Hz), as shown in Figure 6, which suggests that the NMR-detectable Na^+ is exchange broadened.

The addition of NaOH to a clear and neutral solution of titanate nanotubes up to the achievement of the atomic ratio $\text{Na}/\text{Ti} = 0.67$, which is the stoichiometric ratio of sodium titanate ($\text{Na}_2\text{Ti}_3\text{O}_7$), determines the abrupt and total precipitation of the nanotubes present in solution. The Na/Ti ratio measured in this precipitate (after dissolving it by H_2SO_4 treatment) was < 0.01 . This low value indicates that the precipitation of titanate nanotubes is accompanied by the release into solution of most of the Na^+ ions. In a different experiment, we increased the Na^+ concentration by successive additions of NaOH to the neutral (pH 7.2) titanate nanotube solution obtained after ultrasound treatment and containing 32 mM TiO_2 . The ^{23}Na NMR spectrum was recorded after each Na^+ addition. In Figure S1 in the Supporting Information the resonance frequency and the half-height line width are plotted against the added Na^+ . A summary of the significant spectral changes is reported in Table 1. In particular, small changes of the ^{23}Na peak area were observed after addition of NaOH to a concentration of about 4 mM, although the peak line width became narrower ($\Delta\nu_{1/2}$ from 390 to 336 Hz) and meanwhile the pH increased from 7.2

Na^+ added [mM]	pH	Na^+ detected [mM]	Na^+ added/ Na^+ detected	$\Delta\nu_{1/2}$ [Hz]
0	7.2	1.47	–	390
3.85	10.5	1.59	0.41	336
5.70	11.1	2.62	0.46	300
7.60	11.4	3.31	0.43	267
9.50	11.6	3.93	0.41	245
12.5	–	5.22	0.42	210
14.4 ^[a]	–	7.03	0.49	180
14.4 ^[b]	–	10.6	0.74	117

Small amounts of a concentrated NaOH solution were added to a titanate nanotube solution (32 mM TiO_2). Na^+ was added as NaOH and detected by NMR spectroscopy. The measurements were carried out about 1 h after NaOH addition. [a] The titanate nanotube solution was milky. [b] After 24 h of incubation. A precipitate was present.

to 10.5. Further NaOH additions (from 3.85 to about 14 mM) increased the detectable Na^+ up to 41–49% of the added Na^+ . At about 14 mM NaOH the solution became slightly cloudy. This solution was incubated at room temperature for 24 h. After this time a precipitate was present and the detectable Na^+ increased to 74% of the added Na^+ . This increase was accompanied by a strong narrowing of the NMR peak (from $\Delta\nu_{1/2} = 180$ to 117 Hz). The strong increase of the ^{23}Na peak area and the decrease of its line width during the incubation period supports the release in solution of free Na^+ ions from nanotube agglomerates formed under these alkaline conditions. A similar behavior was observed in another experiment on back titration with HCl (see Figure S1 and Table 2). In this

Table 2. Back titration of an alkaline solution of titanate nanotubes with HCl.

HCl _{added} [mM]	pH	Na^+ detected [mM]	$\Delta\nu_{1/2}$ [Hz]
0	11.6	3.75	260
2.6	11.3	3.60	262
5.2	10.3	3.62	237
8.8	7.6	3.93	198
9.8	7.2	4.53	176
10.9	6.7	4.62	158
11.9	5.3	5.12	137
2.9	4.3	5.36	124
13.9	3.3	5.43	112
14.9 ^[a]	3.0	11.0	28
26.0 ^[b]	2.5	12.1	30

Small amounts of a concentrated HCl solution were added to a titanate nanotube solution (32 mM TiO_2) previously made alkaline by addition of 10 mM NaOH. The measurements were carried out about 1 h after HCl addition. [a] A gel phase was present. [b] A precipitate was present.

case the starting sample was a clear and stable solution of nanotubes containing 32 mM TiO_2 , to which NaOH was added up to 10 mM final concentration. Successive additions of 0.5 mM HCl were made to this sample. After a total addition of 10 mM HCl the pH was around neutrality, the half-peak height decreased from 270 to 176 Hz, and a small change of the ^{23}Na detectable by NMR spectroscopy was observed (the peak area is almost constant, as shown in Figure S1). Successive additions of HCl from neutrality to acidic conditions determined a slight increase of the amount of detectable ^{23}Na , which abruptly increased around pH 3.0 at which the nanotubes underwent aggregation and precipitation.

The observed behavior can be explained satisfactorily by assuming a three-site exchange dynamics for Na^+ . The first site (site 1) is the aqueous bulk solution. The second site category (site 2) are the sites for which Na^+ is bound to titanate nanotubes but undergoes fast exchange with free Na^+ . The Na^+ detectable by NMR spectroscopy is the sum of the population in these two sites (i.e. the detected signal is the weighted average of the individual signals of Na^+ in sites 1 and 2). Na^+ in the third site (site 3) is NMR silent because it is strongly immobilized and the exchange frequency with Na^+ in sites 1 and 2 is low with respect to the NMR frequency timescale. The added Na^+ at first saturates the high-affinity sites 3 so that the

peak area does not increase. Upon adding more Na^+ , this ion is shared between sites 1 and 2 according to the average affinity of each site and a fast exchange regime holds for these two sites. Titanate nanotube precipitation is accompanied by a sudden free Na^+ increase.

H^+ added as HCl to the Na^+ -loaded titanate nanotubes first displaces Na^+ in site 2 (so that the signal gets narrower but is constant in its area). More concentrated H^+ competes with Na^+ in site 3 and the area of the detected signal increases as well. These results are in accord with the report by Suetake et al.,^[26] who suggested that in solid titanate nanotubes two states of Na^+ should exist (Na^+ strongly and weakly bound). However, for the first time the experiments were performed in clear and homogeneous solutions, so we had to take into account the fast ion exchange with the aqueous phase. In the soluble titanate nanotubes the strongly bound Na^+ (not NMR detectable) does not exchange with the aqueous phase, thus suggesting that the layered inner tubular structure is scarcely accessible. Confinement of Na^+ in titanate nanotubes is confirmed by conductivity measurements. In fact, according to the above-reported data, the titanate nanotubes washed exhaustively with high-purity water and then sonicated contained 0.1 M titanium and were characterized by a Na^+/Ti ratio as high as 0.083. The conductivity values of these solutions were below 2–3 μS . Conversely, assuming all the Na^+ ions to be free, the expected conductivity should be at least one order of magnitude higher.

2.5. Titanate Nanotube Absorption Edge

UV/Vis spectra of nanotube aqueous solutions were used to calculate the energy bandgap. We used titanate nanotube aqueous solutions because the light scattered by these solutions is negligible, as also indicated in Figure 4. The E_g value calculated according to Tauc et al.^[27] was 3.94 eV (the details of the procedure are reported in the Supporting Information and the Tauc plot is shown in Figure S2). The E_g value is slightly higher than the published one.^[28] However, all the reported data obtained up to now concern solid nanotubes, which should present interfacial differences with respect to the solubilized ones, as suggested by the different hydrophilicity. In particular, the surface order state was suggested to play a role in the bandgap value.^[29] NMR data indicate a high surface density of Na^+ binding sites in solubilized titanate nanotubes and suggest that a structural change, accompanied by Na^+ release, induces precipitation.

2.6. Raman Spectra of Titanate Nanotube Solutions

Raman spectra of titanate nanotubes in aqueous solution were obtained from the air-exposed surface of a specimen in a quartz cuvette (Figure 7, trace B). Dried titanate nanotube samples (Figure 7, trace A) were obtained by deposition of drops of the same solution on a quartz slab and drying under mild vacuum conditions. The Raman spectrum of dried titanate nanotubes shows a set of bands peaking at about 276, 290, 388, 448, 639, 668, 706, 824, and 924 cm^{-1} . The relative intensi-

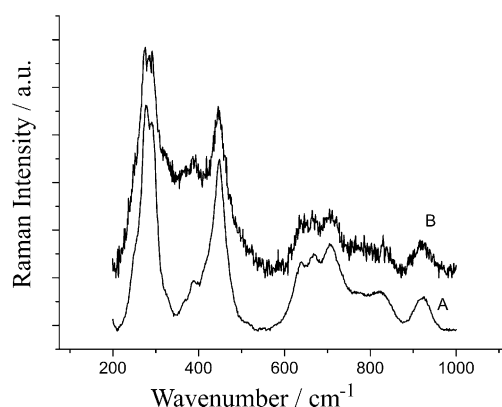


Figure 7. Raman spectra of dried titanate nanotubes (trace A) and titanate nanotube aqueous solution (trace B).

ties and the widths of these bands are consistent with published literature data.^[30–35] In particular, the strong and broad band consisting of at least two components, the main one peaking near 276 cm^{-1} and a shoulder with peak at about 288 cm^{-1} (see Figure 7, trace A), can be assumed to be a key indicator of the formation of the nanotube phase, as pointed out by Morgan et al.^[36] The Raman spectrum of the aqueous solution of titanate nanotubes acquired under the same conditions (Figure 7, trace B) is similar to that of dried titanate nanotubes. However, it is less structured and the relative intensity of some peaks appears to be changed. In particular, the Raman bands occurring in the region between 200 and 400 cm^{-1} are overlapped to a broad spectral bump, which can be attributed to a density of vibrational states. The presence of this feature reflects the disordered nature of the nanostructures. Notwithstanding the broadening in the low-wavenumber region, sharp peaks at 276, 290, 388, and 448 cm^{-1} can be clearly identified. The spectral region at higher wavenumber is essentially similar to that of dried titanate nanotubes (peaks at 639, 668, 704, 820, and 926 cm^{-1}).

A comparison of the relative intensity of the spectra of the dried titanate nanotubes and the aqueous titanate nanotube solution was performed by using the band at about 282 cm^{-1} as reference. This band is assigned to the Ti–O–Ti stretching, which is expected to be scarcely affected by the aqueous phase. In this way we can observe that the band at about 704 cm^{-1} (706 cm^{-1} in the dried sample) decreases in intensity and probably shifts to a lower wavenumber (however, this shift is close to the instrument spectral resolution). This band is assigned to surface Ti–O–Na vibration^[34] and its decrease confirms the presence of exchangeable Na^+ .

3. Conclusions

Titanate nanotubes that are highly soluble in water have been obtained. Positive outcomes for all the applications of titanate nanotubes in the homogeneous phase are expected. We obtained some insights into the distinctive properties of titanate nanotubes in aqueous solution. In particular, reversible exchange of Na^+ was observed. Both fast and slow exchange re-

gimes are present, thus indicating different families of Na^+ binding sites. Raman data confirm the presence of exchangeable Na^+ . Although the morphological characterization of water-soluble titanate nanotubes shows that they have a shape comparable to the solid titanate nanotubes obtained by other authors, the bandgap energy is higher. As the bandgap value is related to the order state of the surface layer,^[29] the higher bandgap value we found suggests a highly ordered state in the surface layer, which is in accord with the strong Na^+ immobilization evidenced by NMR data and with the strong interaction with water molecules that results in the unusual hydrophilicity.

Experimental Section

Structure Characterization of Titanate Nanotubes

Absolute sizes and shapes of the solubilized material were determined by using both TEM and AFM. A drop of clear solution obtained after sonication (4 mM TiO_2) was diluted 1:1000 in distilled water and then deposited on a polyacetate film supported by a copper grid for TEM observations, carried out with a Tecnai G² TEM instrument (FEI, The Netherlands) working at 100 kV. AFM measurements were performed with a ThermoMicroscopes-Veeco CP instrument (Sunnyvale, CA), equipped with an intermittent contact head and 5 and 100 μm scanners, on diluted titanate nanotube solutions deposited on mica sheets. The images were acquired using the tapping mode technique.

Optical Characterization and Bandgap Calculation

The absorbance of TiO_2 nanoparticles and titanate nanotube solutions was obtained by a Varian Cary 50 spectrophotometer. The absorption coefficient α (cm^{-1}) was calculated from the absorbance A as: $\alpha = (A \times 2.3)/d$, in which d is the optical path length. The E_g value of the titanate nanotubes was obtained from the intercept of the Tauc plot^[27] according to the relationship [Eq. (1)]:

$$\alpha = C(h\nu - E_g)^\gamma \quad (1)$$

in which C is a constant and γ is 0.5 for a permitted direct transition.

NMR Experiments

²³Na NMR spectra of titanate nanotubes (79.39 MHz, $\text{H}_2\text{O}/\text{D}_2\text{O}$ 9:1, 25 °C) were recorded with an MSL Bruker instrument by using standard acquisition routines. The instrumental carrier frequency was arbitrarily set to 0 and used as reference for chemical shift. The stability of this frequency during the experimental time was controlled by taking 1 mM Na^+ buffered at pH 7.0 as chemical-shift reference. The carrier frequency drift was negligible during the experimental time. Aqueous solutions of the as-prepared titanate nanotubes were placed in 5 mm NMR tubes and titrations were performed by adding NaOH or HCl as described in Section 2. $1/T_2$ values were obtained from the half-height line width of the ²³Na resonance if the contribution of $1/T_2^*$ was negligible, otherwise the Carr–Purcell–Meiboom–Gill pulse sequence was utilized. Free induction decay processing and line-shape analysis were performed with Topspin software (Bruker, Karlsruhe, Germany).

Raman Experiments

For Raman measurements a microsampling apparatus (Horiba Jobin–Yvon model Labram HR) was used. The system, equipped with an Olympus microscope mounting objectives of different magnification (e.g. 10, 50, 80, and 100 \times), consisted of a He–Ne laser and a narrow-band notch filter. A spectrograph of 80 cm focal length was used. Raman spectra were excited at room temperature by means of the 632.8 nm emission line (about 3 mW power, measured at the exit of the objective) and were detected by a charge-coupled device (1024 \times 256 pixels), cryogenically cooled by liquid nitrogen. The detection limit on the side of low wavenumber, due to the notch filter, was about 200 cm^{-1} . The best Raman spectra were collected by the long-working-distance 80 \times objective. The focused laser spot had an apparent diameter of about 1–2 μm , and the spectral resolution was about 2 cm^{-1} .

Synthesis of Nanotubes and Preparation of Their Aqueous Solutions

Titanate nanotubes were prepared according to the alkaline hydrothermal method of Kasuga et al.^[21] but slightly modified. In a typical synthesis procedure, anatase powder (200 mg) in 10 M NaOH (10 mL) was heated (110 °C, 48 h) in a PTFE vial under gentle mixing. The white powder obtained at the end of this step contained agglomerates as large as 4–5 mm. The flocky sediment (initial volume about 3 mL) was washed exhaustively as follows: addition of distilled water (50 mL), gentle shaking (5 min), and separation by sedimentation (5 min). This washing step was repeated many times to achieve a final pH value between 6 and 7 and a specific conductivity below 20 μS . As the washing step was repeated, the sediment decreased in volume and at the end of the process it looked like a heavy sandy material. According to the UV/Vis spectra (see below) the supernatants did not contain measurable amounts of TiO_2 . The residual material recovered at the end of the washing step was dried at 65 °C and $P < 1 \times 10^{-2}$ Torr for 24 h. The washed and dried sandy material was dispersed in water (50 mL). The turbid powder dispersion was sonicated at 65 °C, 400 W power (ULTRASONIC 28x cleaner, Neytech, Yucaip, CA). A small amount of the suspension was sampled at various times for the absorbance measurements and after 5 min of centrifugation was diluted with distilled water. The absorbance of the diluted solutions was recorded at 245 nm. The sonication time lasted at least 40 h.

Stability tests based on the spectral characteristics were performed on the titanate nanotube solutions. No significant change was observed even after 1 year of storage in the dark at room temperature.

Synthesis of TiO_2 Nanoparticles

TiO_2 nanoparticles were prepared by the method of Pottier et al.^[37] but slightly modified. In particular, TiCl_4 was perfused very slowly in distilled water under vigorous stirring, keeping the temperature of the reaction mixture as low as possible by an ice bath. The solution containing TiO_2 nanoparticles was dialyzed against 1 mM HCl to avoid nanoparticle precipitation.

Determination of Titanium Content

The amount of titanium present in solution was determined after destruction of TiO_2 structures (105 °C, 96% H_2SO_4 , 48 h). The titanil ions so obtained were converted into peroxy-titanates by oxidation with hydrogen peroxide (0.5 M). The titanium concentration was

calculated from the optical absorbance of peroxy-titanates:
 $\lambda_{\max}(\epsilon) = 420 \text{ nm } (690 \text{ mol}^{-1} \text{ L cm}^{-1})$.^[25]

Acknowledgements

The authors thank Giuseppe Tognon for the TEM images.

Keywords: cation confinement · interfaces · nanotubes · NMR spectroscopy · Raman spectroscopy

- [1] D. V. Bavykin, J. M. Friedrich, F. C. Walsh, *Adv. Mater.* **2006**, *18*, 2807–2824.
- [2] P. Hoyer, *Langmuir* **1996**, *12*, 1411–1413.
- [3] H.-H. Ou, S.-L. Lo, *Sep. Purif. Technol.* **2007**, *58*, 179–191.
- [4] P. V. Kamat, *J. Phys. Chem. C* **2012**, *116*, 11849–11851.
- [5] P. Roy, S. Berger, P. Schmuki, *Angew. Chem.* **2011**, *123*, 2956–2995; *Angew. Chem. Int. Ed.* **2011**, *50*, 2904–2939.
- [6] Y. Tang, D. Dong, Y. Lai, Y. Shen, Y. Zhang, Y. Huang, J. Tao, C. Lin, Z. Dong, Z. Chen, *J. Mater. Chem.* **2010**, *20*, 10169–10178.
- [7] K.-S. Mun, S. D. Alvarez, W.-Y. Choi, M. J. Sailor, *ACS Nano* **2010**, *4*, 2070–2076.
- [8] N. K. Shrestha, J. M. Macak, F. Schmidt-Stein, R. Hahn, C. T. Mierke, B. Fabry, P. Schmuki, *Angew. Chem.* **2009**, *121*, 987–990; *Angew. Chem. Int. Ed.* **2009**, *48*, 969–972.
- [9] C. McCullagh, N. Skillen, M. Adams, P. K. J. Robertson, *J. Chem. Technol. Biotechnol.* **2011**, *86*, 1002–1017.
- [10] Y. Ide, M. Matsuoka, M. Ogawa, *J. Am. Chem. Soc.* **2010**, *132*, 16762–16764.
- [11] W. Hou, Z. Liu, P. Pavaskar, W. H. Hung, S. B. Cronin, *J. Catal.* **2011**, *277*, 149–153.
- [12] M. Anpo, *Pure Appl. Chem.* **2000**, *72*, 1787–1792.
- [13] S. T. Hussain, A. Siddiq, *Int. J. Sci. Techn.* **2011**, *8*, 351–362.
- [14] B. C. Viana, O. P. Ferreira, A. G. Souza Filho, C. M. Rodrigues, S. G. Moraes, J. Mendes Filho, O. L. Alves, *J. Phys. Chem. C* **2009**, *113*, 20234–20239.
- [15] C. Von Wilmowsky, S. Bauer, R. Lutz, M. Meisel, F. W. Neukam, T. Toyshima, P. Schmuki, E. Nkenke, K. A. Schlegel, *J. Biomater. Mater. Res. Part B* **2009**, *89*, 165–171.
- [16] A.-L. Papa, L. Maurizi, D. Vandroux, P. Walker, N. Millot, *J. Phys. Chem. C* **2011**, *115*, 19012–19017.
- [17] A. Kodama, S. Bauer, A. Komatsu, H. Asoh, S. Ono, P. Schmuki, *Acta Biomater.* **2009**, *5*, 2322–2330.
- [18] G. K. Mor, O. K. Varghese, M. Paulose, C. A. Grimes, *Adv. Funct. Mater.* **2005**, *15*, 1291–1296.
- [19] H. Shin, D. K. Jeong, J. Lee, M. M. Sung, J. Kim, *Adv. Mater.* **2004**, *16*, 1197–1200.
- [20] T. Kasuga, M. Hiramatsu, A. Hoson, T. Sekino, K. Niihara, *Langmuir* **1998**, *14*, 3160–3163.
- [21] T. Kasuga, M. Hiramatsu, A. Hoson, T. Sekino, K. Niihara, *Adv. Mater.* **1999**, *11*, 1307–1311.
- [22] D. V. Bavykin, J. M. Friedrich, A. A. Lapkin, F. C. Walsh, *Chem. Mater.* **2006**, *18*, 1124–1129.
- [23] C. Ratanatawanate, J. Yu, C. Zhou, J. Zheng, K. J. Balkus, *Nanotechnology* **2011**, *22*, 065601–06565.
- [24] K. Vasilev, Z. Poh, K. Kant, J. W. Chan, A. Michelmore, D. Losic, *Biomaterials* **2010**, *31*, 532–540.
- [25] D. Snell, C. T. Snell, in *Colorimetric Methods of Analysis, 3rd Ed., Vol. 2*, Van Nostrand, New York, **1949**, pp. 438–439.
- [26] J. Suetake, A. Y. Nosaka, K. Hodouchi, H. Matsubara, Y. Nosaka, *J. Phys. Chem. C* **2008**, *112*, 18474–18482.
- [27] J. Tauc, A. Grigorovici, A. Vancu, *Phys. Status Solidi* **1966**, *15*, 627–637.
- [28] H. Tokudome, M. Miyauchi, *Chem. Lett.* **2004**, *33*, 1108–1109.
- [29] X. Chen, L. Liu, P. Y. Yu, S. S. Mao, *Science* **2011**, *331*, 746–750.
- [30] T. Gao, H. Fjelvig, P. Norby, *Inorg. Chem.* **2009**, *48*, 1423–1432.
- [31] B. C. Viana, O. P. Ferreira, A. G. Souza Filho, A. A. Hidalgo, J. Mendes Filho, O. L. Alves, *Vib. Spectrosc.* **2011**, *55*, 183–187.
- [32] T. Beuquier, M. Richard-Plouet, L. Brohan, *J. Phys. Chem. C* **2010**, *114*, 7660–7665.
- [33] P. Haro-González, M. Pedroni, F. Piccinelli, L. L. Martin, S. Polizzi, M. Giarola, G. Mariotto, A. Speghini, M. Bettinelli, I. R. Martin, *J. Lumin.* **2011**, *131*, 2473–2477.
- [34] S.-J. Kim, Y.-U. Yun, Y.-J. Oh, S. H. Hong, C. A. Roberts, K. Routray, I. E. Wachs, *J. Phys. Chem. Lett.* **2010**, *1*, 130–135.
- [35] D. V. Bavykin, M. Carravetta, A. N. Kulak, F. C. Walsh, *Chem. Mater.* **2010**, *22*, 2458–2465.
- [36] D. L. Morgan, H.-W. Liu, R. L. Frost, E. R. Waclawik, *J. Phys. Chem. C* **2010**, *114*, 101–110.
- [37] A. Pottier, S. Cassaignon, C. Chaneac, F. Villain, E. Tronc, J. P. Joliver, *J. Mater. Chem.* **2003**, *13*, 877–882.

Received: March 25, 2013

Published online on June 28, 2013